Ammonia recovery from organic nitrogen in synthetic dairy manure with a microbial fuel cell

McKenzie Burns[1] and Mohan Qin[1,2]*

1. *Department of Civil and Environmental Engineering, University of Wisconsin–Madison, Madison, Wisconsin 53706, USA*
2. *Environmental Chemistry and Technology Program, University of Wisconsin–Madison, Wisconsin 53706, USA*

* Corresponding author. E-mail: mohan.qin@wisc.edu

Abstract

Increasing pressures on the animal and cropland agriculture sectors have led to the realization of problems with animal waste management and ammonia-based fertilizer supply. Bioelectrochemical systems (BES) are a new-age technology that offer a way to address these problems. Microbial fuel cells (MFCs), one type of BES, are traditionally used for electricity generation from microbial degradation of organic matters, but can also be used to recover nutrients from wastes simultaneous with treatment. This research investigated an MFC for ammonia recovery from the organic nitrogen (orgN) fraction of synthetic dairy manure, using the simple amino acid glycine as the orgN source. We used five different synthetic manure compositions to determine their effects on MFC performance, and found minimal sacrifices in performance under orgN conditions when compared to the base condition without orgN. The MFC achieved greater than 90% COD removal in all orgN conditions. Nitrogen (N) removal efficiencies of between 40% and 60% were achieved in orgN conditions, indicating that organic nitrogen can be used as the substrate for ammonia mineralization and further recovery as fertilizer. In addition, we found the MFC was largely populated by electrogenic organisms from the phyla Bacteroidota, Firmicutes, Proteobacteria, and Halobacterota, with organisms in both Bacteroidota and Firmicutes capable of N mineralization present. Lastly, we found that in conditions where orgN is scarce and the only N source provided, microbes preferentially degraded organic matter from other dead organisms, especially as an N source. This increases the concentration of N in the MFC system and introduces important operational constraints for MFCs operated for ammonia recovery from orgN.

Keywords: Microbial fuel cells, organic nitrogen, ammonia recovery, microbial nitrogen mineralization, manure remediation

Graphical Abstract

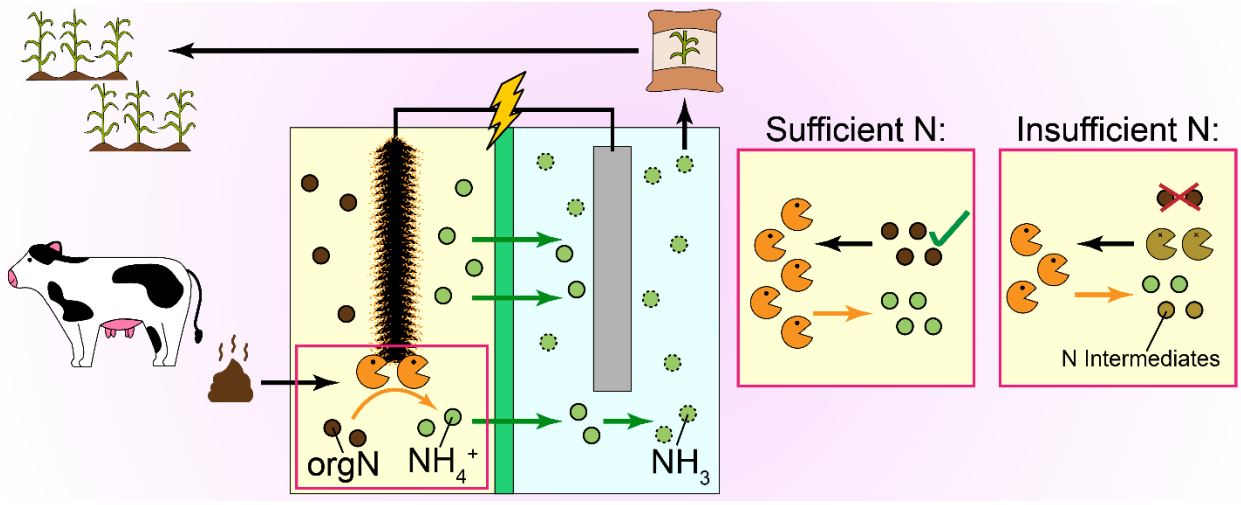

1. Introduction

Global population growth continues to drive demand for food higher than ever before, putting excess pressure on both crop and livestock agriculture sectors. Nitrogenous fertilizers are among the most widely used stimulants for crop growth and yield, with the majority of fertilizer nitrogen (N) in the form of ammonia (NH_3) (Wang et al., 2021). More than 96% of this ammonia is produced via the Haber-Bosch process, which is a high pressure, high temperature thermochemical reaction combining atmospheric N_2 and H_2 (Smith et al., 2020). The Haber-Bosch process is largely powered by fossil fuels, and greenhouse gas emissions from this process are responsible for nearly 1% of global emissions (Wang et al., 2021). With the demand for NH_3-based fertilizers expected to further increase, sustainable NH_3 production represents an increasingly important challenge.

Simultaneously, increasing production in the livestock agriculture sector has led to exponential growth in both the number and size of animal feeding operations nationally. In 2020, the United States Environmental Protection Agency (US EPA) reported nearly 21,000 concentrated animal feeding operations (CAFOs) throughout the country (EPA, 2022). Under The Clean Water Act, CAFOs are operations which house confined animals for more than 45 days per year and meet specified size thresholds, for example, more than 1000 beef cattle or 700 dairy cows, or discharge manure or wastewater directly into a waterway (EPA, 2008; Long et al., 2018). CAFOs are under pressure to become more environmentally sustainable. Many issues stem from the mismanagement of livestock manure, a mixture of animal feces, urine, and other system by-products (e.g., wash waters, waste feed). Manure constituents, including nutrients, pathogens, and organic matter, can be lost to the environment, degrading both surface and

ground water quality, contributing to climate change, causing nuisance odors, and creating environmental and human health issues.

Current manure remediation techniques include direct land application and microbiological processing; however, the unique properties of animal manures complicate these approaches. For example, direct land application of manure is often limited to geographic areas immediately surrounding the CAFO of origin. Manure properties like high water content and low nutrient density increase transportation costs, restricting effective use of manure. Additionally, the majority of nutrients in manure are in organic forms, which are unusable to plants without prior mineralization to inorganic forms. While this mineralization can happen *in situ* once manure is applied to croplands, it is a slow, microbial process that is difficult to control. The combination of delayed fertilization effects and challenging transport of manure often leads to excess manure application in one geographic area. This results in localized manure nutrient loading to exceed agronomic need, increasing nutrient losses to the environment and reducing nutrient use efficiency. Microbiological processes, such as anaerobic digestion (AD) and composting, are somewhat effective at treating the organic load of animal manures; however, these remediation techniques do not address the high concentrations of nutrients in manure. Oftentimes, the orgN and NH_3 contained in manure inhibits the activity of microorganisms in AD, and N losses in composting due to NH_3 off gassing typically exceed losses from conventional manure storage (Hansen et al., 1998; Pardo et al., 2015). Additionally, methane gas can leak from these processes, increasing the potential for greenhouse gas emissions. These shortcomings support the need for development of new technologies capable of both treating the organic load of manure and recovering nutrients in readily usable forms. Bioelectrochemical systems (BES) are a relatively new approach to waste treatment, and when applied to manure

remediation, BES optimized for nutrient recovery offer a unique solution to both NH_3 production and manure management issues.

BES are traditionally categorized as microbial electrolysis cells (MECs), microbial desalination cells (MDCs), or microbial fuel cells (MFCs) depending on the desired treatment and output (Wang and Ren, 2013; Kelly and He, 2014; Lu and Ren, 2016; Gul and Ahmad, 2019; Chu et al., 2020). Generally, BES operation combines principles of microbiology and electrochemistry to engineered systems which utilize microbe-mediated degradation reactions to treat waste streams and produce value-added products, such as electricity, hydrogen fuel, or concentrated chemical solutions (Gul and Ahmad, 2019; Kelly and He, 2014; Lu and Ren, 2016). When an ion exchange membrane is placed between the anode and cathode chambers of an MFC, ion transport across the membrane is enabled by simultaneous current generation. Therefore, MFCs are considered an efficient chemical recovery system, especially for recovering NH_3 from waste streams (Kelly and He, 2014; Zhang et al., 2014; Rodríguez Arredondo et al., 2015; Rodríguez Arredondo et al., 2017). In MFCs operated for NH_3 recovery, free ammonium (NH_4^+) in the anode chamber is transported to the cathode chamber across a cation exchange membrane (CEM) via both electromigration and diffusion (Liu et al., 2016). The NH_4^+ is then converted to NH_3 due to the high pH of the catholyte and can be recovered via air stripping. This recovery is dependent on an abundance of NH_4^+ in the anolyte, which is heavily influenced by the anolyte composition.

Although MFCs have been demonstrated to effectively recover NH_4^+ from wastewater, little research has been conducted related to anodic conversions of organic nitrogen (orgN) to NH_4^+ prior to recovery. Previously, substrates used in MFC research have contained minimal orgN, and in the cases where N recovery has been studied, the anolyte N is typically already in

110 the form of NH_4^+ when fed to the MFC. As such, NH_3 recovery is solely the product of NH_4^+
111 transport from anode to cathode chamber to balance the influx of electrons in the cathode
112 chamber. The majority of N in animal manures is as orgN, which would first need to be
113 converted to NH_4^+ via N mineralization before transport across the CEM and recovery in the
114 catholyte. Microbial N mineralization can be cultivated in the biological anode of the MFC under
115 the proper conditions. It is important to study the impact that this additional step of N
116 mineralization will have on MFC performance if MFCs are to be used as future manure
117 remediation and NH_3 recovery technologies.

118 In contribution to the application of MFCs as chemical resource recovery mechanisms,
119 this research investigated MFC operation for NH_3 recovery from orgN in a synthetic dairy
120 manure substrate. Glycine, a simple amino acid, was used as a model orgN substrate. Multiple
121 electrolyte compositions were evaluated to determine their impacts on overall MFC performance,
122 the orgN to NH_4^+ conversion pathway, and NH_4^+ removal from the anolyte. This work focused
123 specifically on anodic processes, and as such, the recovery of NH_3 gas was outside the scope;
124 however, this has been studied in detail elsewhere (Kuntke et al., 2012; Kim et al., 2021). The
125 objectives of this work were to (1) determine if it is possible for microbes in an MFC anode to
126 mineralize orgN to NH_4^+, (2) investigate the optimal MFC conditions for N mineralization and
127 removal from the anolyte, and (3) propose potential degredation pathways for simple orgN
128 compounds and acetate in an MFC operated for NH_3 recovery from orgN.

129 **2. Materials and Methods**

130 *2.1. MFC setup and operation*

The MFC used in this study was a two-chamber design with a biological anode and a chemical cathode, separated by a cation exchange membrane (Logan et al., 2006; Cord-Ruwisch et al., 2011; Kuntke et al., 2012; Qin and He, 2014; Qin et al., 2016; Yang et al., 2017; Ye et al., 2019) (Figure 1). Dual-chamber MFC operation relies on a biological anode cultivated with exoelectrogenic microbes and fed with the wastewater as the anolyte (Logan et al., 2006). As the microbes degrade the organic matter available in the anolyte, extracellular electrons are produced and sent to the cathode, where they are consumed by a reduction reaction (Logan et al., 2006). In this study, we cultivated for microbial N mineralization in the anode chamber, and selected varying conditions to investigate the optimization of N mineralization on the anode and NH_4^+ transport to the cathode across the CEM, as shown in Figure 1.

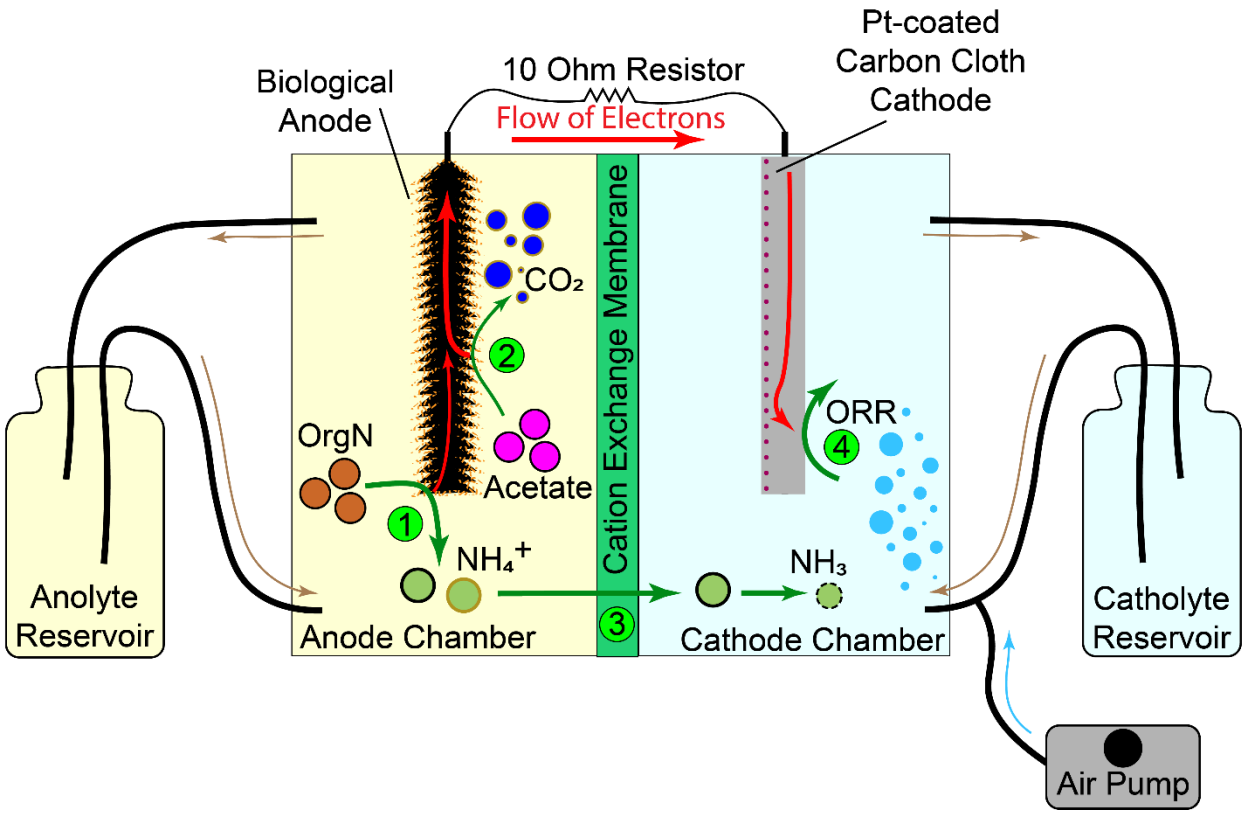

Figure 1. Schematic of the microbial fuel cell (MFC) set up. The essential processes and reactions occurring during operation include microbial degradation of acetate (1) and organic nitrogen (orgN) (2), transport of NH_4^+ across the cation exchange membrane (CEM) (3), and consumption of electrons at the cathode by the oxygen reduction reaction (ORR) (4). Two carbon fiber brushes were entwined with titanium wire for the anode and the cathode consisted of a platinum-catalyst treated carbon cloth supported with metal mesh and wrapped in titanium wire. Electrodes were connected via a 10 Ω resistor and a voltage multimeter recorded the potential drop across the resistor. An air pump was connected in-line with the catholyte recirculation system to deliver oxygen to the cathode to fuel the ORR. Electrolyte solutions were replaced at the beginning of each experimental cycle, such that the hydraulic retention time for each cycle was 48h. Chemical components added as part of anolyte feed solution(s) are indicated in black outlines and chemical components produced through microbial metabolism are indicated in brown outlines.

A stacked-plate MFC was constructed with two endplates (McMaster-Carr, Chicago, IL, USA) and three inner rubber frames (McMaster-Carr, Chicago, IL, USA). The rubber frames were sandwiched between the endplates to create the internal chamber volumes of 200 mL and 100 mL for the anode and cathode chambers, respectively. Electrode chambers were separated by a cation exchange membrane (CMI 7000S, Membranes International, Inc., Ringwood, NJ, USA). The anode chamber housed two carbon fiber brushes (The Mill-Rose Company, Mentor, OH, USA) as the electrode, and was inoculated with mesophilic anaerobic digestion sludge from Nine Springs Wastewater Treatment Plant (Madison, WI, USA). A carbon cloth cathode (area = 39 cm^2, Zoltek Companies, Inc., Bridgeton, MO, USA) was coated with a platinum-carbon

165 catalyst (10% wt/wt Pt/C, Fuel Cell Earth, Woburn, MA, USA) (Zhang et al., 2013; Qin et al.,
166 2017). Electrolyte solutions were continuously recirculated at a rate of 76 mL min^{-1} between the
167 internal chambers and external reservoirs (500 mL total anolyte volume and 600 mL total
168 catholyte volume) for hydraulic retention times of 48h per experimental cycle. This recirculation
169 rate allowed for the entire internal chamber volume to be replaced every 1-3 minutes, ensuring
170 adequate mass transfer conditions were sustained.

171 *2.2. Experimental Conditions*

172 Experiments were conducted in five stages corresponding to five different electrolyte
173 conditions: the original acetate and NH_4Cl feeding condition ("Original"), a glycine and
174 phosphate buffer anolyte condition ("GP"), a glycine and reduced phosphate buffer condition
175 ("GP_{red}"), a glycine only anolyte condition ("GO"), and an ultra-low glycine only anolyte
176 condition ("GO_{low}") (Table 1). For all electrolyte conditions, 0.024 M sodium acetate served as
177 the main source of organic carbon (Angenent and Sung, 2001; Qin et al., 2017). Detailed notes
178 on trace solution composition are provided in the SI. The simple amino acid glycine was used as
179 the source of orgN in these experiments. Different concentrations of phosphate buffer solution
180 (PBS) were used as the catholyte, based on the electrolyte condition under investigation (Table
181 1). In later stages of the experimental work, the concentration of catholyte PBS was decreased in
182 order to more closely mimic the conductivity of typical tap water while still yielding significant
183 control over specific solution composition. Other chemical components of the electrolyte
184 solutions varied throughout the study in correspondence with the purpose for studying the given
185 condition, as described in Table 1 and in the SI. Within each electrolyte condition, data from at
186 least three, 48h cycles (determined as the time required for current density to drop below ~ 0.25
187 A m^{-2} cathode area, the chosen threshold for significant COD removal) was collected. Chemicals

used for preparation of the stock and electrolyte solutions were purchased from Carolina Chemical (Charlotte, NC, USA), Alfa Aesar (Thermo Fisher Scientific, Tewksbury, MA, USA), and Sigma-Aldrich (Merck KGaA, Darmstadt, Germany). Anolyte solutions were purged with N_2 gas for ~ 15 minutes immediately prior to use.

Table 1. Electrolyte compositions for each condition and a brief description of the purpose for investigating each electrolyte condition. Exact compositions for the stock, trace, and phosphate buffer (PBS) solutions can be found in Table S1.

Electrolyte Condition	**Purpose**	**Anolyte Composition**[†]	**Catholyte Composition**
Original feeding conditions ("Original")	Facilitated microbial growth on anode and collection of baseline cell performance	0.56 M NH_4^+-N 0.01 M stock 0.1 M PBS	0.02 M PBS
Glycine **P**hosphate Anolyte ("GP")	Introduced glycine as orgN source	0.14 M glycine-N 0.01 M stock 0.02 M PBS	0.02 M PBS
Glycine and **Red**uced **P**hosphate ("GP_{red}")	Investigated MFC capacity to self-buffer under orgN conditions via removal (anolyte) and reduction (catholyte) of the buffer solution	0.14 M glycine-N 0.01 M stock	0.002 M PBS
Glycine **O**nly Anolyte ("GO")	Investigated orgN degredation capability in absence of readily available inorganic N-source	0.14 M glycine-N 0.01 M stock*	0.002 M PBS
Ultra-**low** **G**lycine **O**nly Anolyte ("GO_{low}")	Investigated MFC performance under ultra-low orgN concentrations	0.005 M glycine-N 0.01 M stock*	0.002 M PBS

[†]Anolyte under all conditions was prepared with 0.024 M sodium acetate and 0.001 M trace solution.

*A separate stock solution without NH_4Cl was prepared and used in place of the original stock solution for these preparations. See Table S1 for further information.

2.3. Analytical Methods

2.3.1. Electrolyte Characterizations

pH and conductivity of electrolyte solutions were measured via electrode probe and benchtop meter (Orion Versa Star Pro, Thermo Fisher Scientific, Waltham, MA, USA). Chemical oxygen demand (COD), total nitrogen (TN) and ammonia nitrogen (NH_3-N, measured as the sum of $NH_{3(aq)}$ and NH_4^+) were measured via standard colormetric methods (COD Digestion Vials High Range, Total Nitrogen Persulfate Digestion Test 'N Tube, and High Range Ammonia Nitrogen AmVer Salicylate Test 'N Tube, Hach, Loveland, CO, USA). The difference in TN and NH_3-N concentrations for individual samples was assumed to be entirely organic nitrogen (orgN) in the form of glycine, although later analysis determined this to be unlikely under certain operative conditions (see section 3.3). Percent removal of nutrients, *R*, was calculated via Eq. 1:

$$R = \frac{C_i - C_f}{C_i} * 100 \quad \text{(Eq. 1)}$$

where C_i is the initial anolyte concentration of the nutrient of interest and C_f is the final anolyte concentration of the nutrient of interest.

2.3.2. MFC Electrochemical Characterization

The current generation was continuously monitored using a data acquisition and logging multimeter system from Keithley Instruments (Tektronix, Inc., Beaverton, OR, USA). The cell was operated with an external resistance of 10 Ohms throughout the study. The current density

was normalized to the area of cathode electrode. For each cycle, the total charge transferred (Q, in Coulombs) between anode and cathode was computed as the area under the current-time curve using the trapezoidal method for approximate integration (Eq. 2):

$$Q = \sum_{i=0}^{n=t_f} \left(\frac{I_t + I_{t+\Delta t}}{2}\right) \Delta t \quad \text{(Eq. 2)}$$

where I_t is the current (in Amperes) at time t, $I_{t+\Delta t}$ is the current (in Amperes) at time $t+\Delta t$, t_f is the final recorded time of the cycle, and Δt is 5 minutes. The total nitrogen removal efficiency (R_N, in mole N mole^{-1} electrons) is a measure of how current was partitioned to drive nitrogen transport from anode to cathode chambers. R_N was calculated via Eq. 3:

$$R_N = \frac{V_{an} F (TN_{i,an} - TN_{f,an})}{Q} \quad \text{(Eq. 3)}$$

where V_{an} is the total volume of anolyte (in L), F is Faraday's constant (96,485 Coulombs per mole of electrons), and $TN_{i,an}$ and $TN_{f,an}$ are the initial and final total nitrogen concentrations in the anolyte (in M), respectively.

2.3.3. Microbial Community Analysis

Microbial community analysis was performed on selected replicates of samples taken during 5 different sampling conditions throughout the study: the inoculant anaerobic digestate ("Inoculant"), after resistance decrease to cultivate for electrogenic organisms ("Initial Electrogens"), after the completion of several experimental cycles with the original acetate and NH_4Cl electrolyte condition ("Original", see Table 1), during and after the experimental cycles in the glycine only electrolyte condition ("GO", see Table 1), and during and after the experimental cycles in the ultra-low glycine only electrolyte condition ("GO_{low}", see Table 1). Samples for microbial community analysis were further divided into three intra-condition

sampling time categories, denoting samples either taken at the start ("Condition Start"), middle ("Mid-Condition"), or end ("Condition End") of the cycles in the relevant electrolyte condition. Sample replicates labeled with "No Time" indicate those collected at only one time within the electrolyte condition cycles.

DNA extraction was performed using the DNeasy PowerSoil Pro Kit (Qiagen, Germantown, MD, USA) per the manufacturer's procedure. DNA samples were sent to the University of Wisconsin—Madison Biotechnology Center (Madison, WI, USA) for 16S rRNA analysis. Sequenced reads were denoised and filtered for quality using the DADA2 program. Resultant amplicon sequence variants (ASVs) were assigned taxonomy according to a Bayesian classifier based on a pre-trained silva database curated to the 16S rRNA amplicon region. Diversity analysis and statistical comparison were performed in R using the "phyloseq" and "DivNet" packages for microbiome analysis (McMurdie and Holmes, 2013; Team, 2022; Willis and Martin, 2022). Alpha diversity of each sample was calculated as the Shannon diversity index, *H*, via Eq. 4:

$$H = -\sum p * \ln p \quad \text{(Eq. 4)}$$

where *p* is the number of appearances of a given operational taxonomic unit (OTU) normalized to the total number of OTU appearances in the sample. Beta diversities were calculated using Bray-Curtis dissimilarity, BC_{ij}, via Eq. 5:

$$BC_{ij} = 1 - \frac{2C_{ij}}{S_i + S_j} \quad \text{(Eq. 5)}$$

where C_{ij} is the lower count of OTU appearances for a given OTU that appears in both samples *i* and *j*, and S_i and S_j are the total number of OTU appearances in each sample *i* and *j*, respectively (Bray and Curtis, 1957).

3. Results and Discussion

3.1. MFC Performance

MFC performance was evaluated at five different conditions: the original acetate and NH_4Cl ("Original") condition to establish the baseline performance, a glycine-phosphate ("GP") and a reduced glycine-phosphate ("GP_{red}") condition to introduce organic nitrogen to the system and to test the MFC's ability to self-buffer, a glycine-only ("GO") condition to test the MFC's ability to operate on only orgN, and an ultra-low glycine only ("GO_{low}") condition to test the MFC performance in an N-limiting environment (Table 1). The anolyte solution compositions represented a synthetic dairy manure, and sequential removal/replacement of various components of the original electrolyte conditions allowed for slow, selective optimization of the microbial anode. MFC performance was evaluated based on pH, conductivity, and total charge transfer per cycle, as well as COD, TN, and NH_3 removal from the anolyte, and total nitrogen removal efficiency.

3.1.1. Electrochemical Performance

Results from the original electrolyte condition were used as a basis for comparison with results from the orgN electrolyte conditions. In the original electrolyte condition, the average pH values of final electrolyte solutions remained neutral at 7.13 ± 0.10 and 7.17 ± 0.03 for anolyte and catholyte solutions, respectively, which was relatively unchanged from the initial solution pH values of 7.03 and 7.28 for anolyte and catholyte solutions, respectively. This indicates stable

acid/base conditions for the entirety of the cycles and condition. For the orgN electrolyte conditions, different patterns in electrolyte pHs were observed (Figure 2a). All of the orgN conditions showed a significant increase in average final catholyte pH; from 7.61 ± 0.07 to 8.97 ± 0.25 for the GP condition, 7.61 ± 0.07 to 9.04 ± 0.15 for the GP_{red} condition, 7.89 ± 0.10 to 8.85 ± 0.02 for the GO condition, and 7.88 ± 0.05 to 9.12 ± 0.07 for the GO_{low} condition. The GP and GP_{red} conditions showed no change from initial to final anolyte pH (7.06 to 7.32 ± 0.24 and 7.82 ± 0.31 to 7.71 ±0.17, respectively). The GO and GO_{low} conditions showed slight decreases from initial to final anolyte pH measurements (7.85 ± 0.12 to 7.40 ± 0.06 and 7.33 ± 0.20 to 6.68 ± 0.04, respectively). The increase in final catholyte pH under orgN conditions is likely due to reduced NH_4^+ transfer, as there is less readily available NH_4^+ in these conditions. Additionally, the decreases in concentrations of catholyte PBS in the GP_{red}, GO, and GO_{low} conditions could result in reduced catholyte buffering capacity and thus the decreases in catholyte pH.

Comparatively, the stagnant nature of the anolyte pH across all conditions is advantageous for current production. Many studies have shown that a neutral anodic pH yields higher current generation in MFCs (Gil et al., 2003; Cheng et al., 2007; Ren et al., 2007; He et al., 2008; Ren et al., 2008; Zhang et al., 2012). Additionally, the stability of anodic pH in the absence of an added buffer solution (as in the GP_{red}, GO, and GO_{low} conditions) indicates that MFCs can successfully operate on decreased added resources and are likely to be more cost effective. He et al. (2008) suggest that bacterial metabolism can act as a buffering system within the anode chamber, as microbes continuously produce weak acids to maintain appropriate pH for life that can buffer the increase in pH resulting from proton transport out of the anode chamber via the CEM. The slight decrease observed from initial to final anolyte pH in GO and GO_{low} conditions is likely due to partial degradation of substrates to organic acids (see section 3.3).

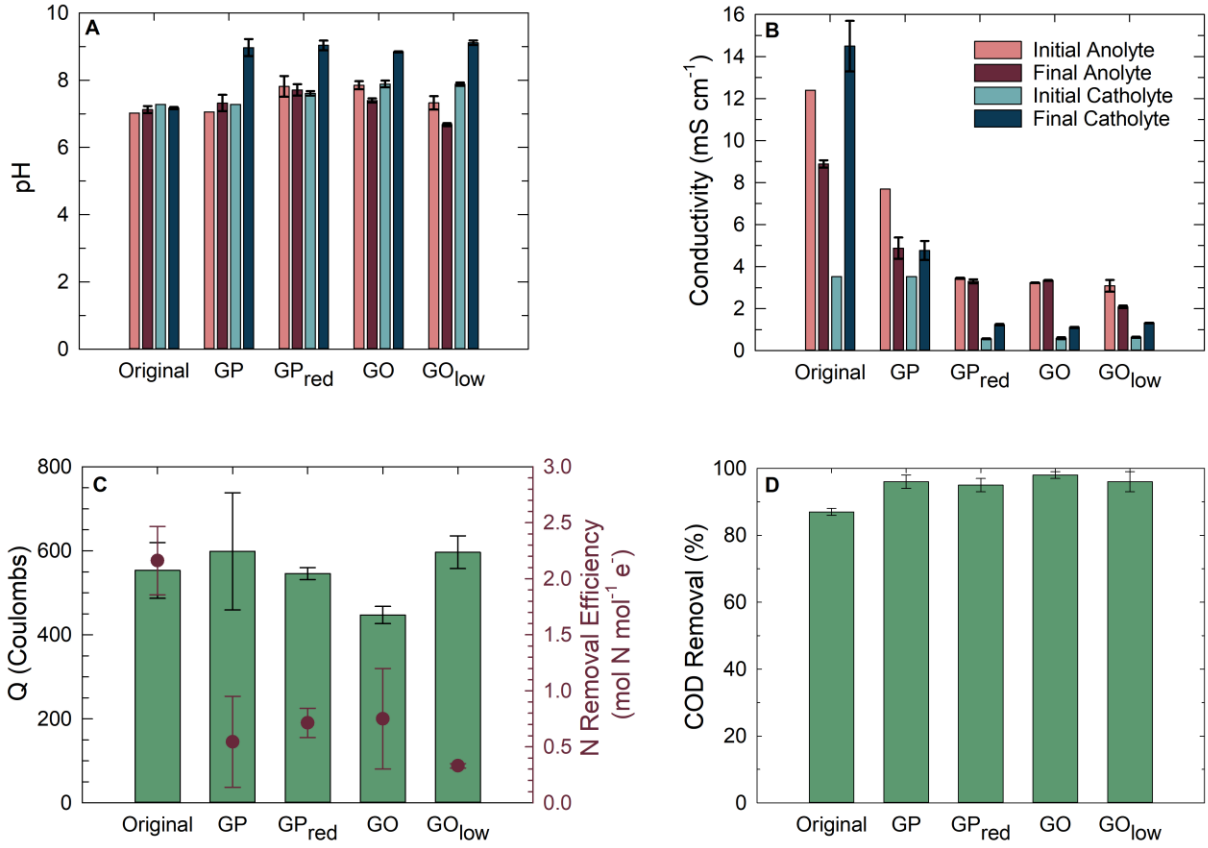

303

304 **Figure 2.** System performance at different feed conditions: the original acetate and NH_4Cl

305 feeding condition ("Original"), a glycine and phosphate buffer anolyte condition ("GP"), a

306 glycine and reduced phosphate buffer condition ("GP_{red}"), a glycine only anolyte condition

307 ("GO"), and an ultra-low glycine only anolyte condition ("GO_{low}"). (A) initial and final pH in

308 anolyte and catholyte, (B) initial and final conductivity in anolyte and catholyte; (C) total charge

309 transfer (Q) and total nitrogen removal efficiency, calculated via Eq. 2, and (D) COD removal

310 efficiency, calculated via Eq. 1.

311

312 The original condition showed a decrease in anolyte conductivity from 12.4 mS cm^{-1} to

313 8.88 mS cm^{-1} and an increase in catholyte conductivity from 3.52 mS cm^{-1} to 14.5 mS cm^{-1} from

initial to final measurements, which supports the occurrence of desired NH_4^+ transport from anolyte to catholyte (Figure 2b). Similar trends in anolyte and catholyte initial and final conductivities were observed for the GP and GO_{low} conditions (from 7.69 mS cm^{-1} to 4.88 mS cm^{-1} in the anolyte and from 3.52 mS cm^{-1} to 4.77 mS cm^{-1} in the catholyte for the GP condition, and from 3.09 ± 0.28 mS cm^{-1} to 2.08 ± 0.06 mS cm^{-1} in the anolyte and 0.634 ± 0.03 mS cm^{-1} to 1.32 ± 0.02 mS cm^{-1} in the catholyte for the GO_{low} condition). The GP_{red} and GO conditions exhibited unchanged anolyte conductivities from initial to final measurements. The catholyte conductivities in the GP_{red} and GO conditions exhibited the increases from initial to final measurements, as seen in other experimental conditions (from 0.57 ± 0.02 mS cm^{-1} to 1.24 ± 0.03 mS cm^{-1} in the GP_{red} condition and from 0.59 ± 0.04 mS cm^{-1} to 1.11 ± 0.03 mS cm^{-1} in the GO condition). The decreases in magnitude of the electrolyte conductivities correspond with decreasing concentrations of available ions, which changed with varied electrolyte compositions outlined in Table 1. In later experimental conditions (GP_{red}, GO, and GO_{low}), the decreased conductivity and corresponding low concentration of ions in the catholyte solutions likely increased the resistance of the solution, introducing important charge transfer constraints. However, there were minimal sacrifices observed in average total charge transfer in these conditions (Figure 2c), and the increases in catholyte conductivity observed from initial to final measurements (Figure 2b) indicate that flow of ions from anode to cathode chambers was not greatly inhibited by the increased resistance of the catholyte.

The average total charge transfer, Q, for almost all electrolyte conditions was between 500 and 600 Coulombs, except for the GO condition, where Q dropped to around 450 Coulombs (Figure 2c). A baseline average maximum current density of 1.44 ± 0.29 A m^{-2} was generated in the original electrolyte condition, and the average maximum current densities recorded for the

orgN cycles were all within the one standard deviation of the baseline (Figure S1). The highest recorded average current density was 1.69 ± 0.31 A m^{-2} in the GO_{low} condition, and the lowest was 1.37 ± 0.01 A m^{-2} in the GP_{red} condition. The Q values and average maximum current densities generated in this study are equal to or greater than those produced in previous MFC research, where the sole focus was electricity production from organic removal in wastes (Pant et al., 2010; Syed et al., 2022). Additionally, our MFC achieved COD removal efficiencies greater than those reported in studies where electricity produciton and organic removal were the only focus and nitrogen removal/recovery was not investigated (see section 3.1.2) (Liu et al., 2004; Rasouli Sadabad and Badalians Gholikandi, 2018; Syed et al., 2022). These findings support our conclusion that nitrogen recovery is an advantageous application of MFC technology (Pant et al., 2010; Kuntke et al., 2012; Kelly and He, 2014; Rodríguez Arredondo et al., 2015; Gude, 2016; Gul and Ahmad, 2019).

3.1.2. Nutrient Removal Performance

Under all electrolyte conditions, the MFC achieved excellent organics removal (measured as COD) efficiencies, at 87% removal in the original condition and above 95% removal for all orgN electrolyte conditions, as shown in Figure 2d. COD removal in this study was higher than what has been previously reported for similar systems (Liu et al., 2004; Rozendal et al., 2009; De Paepe et al., 2020; Syed et al., 2022). This may suggest that more complex substrates and cultivation for N mineralizing organisms provide compounding advantages, however, more research is needed to definitively substantiate this statement. Total nitrogen removal efficiency, R_N, decreased from 2.16 ± 0.31 mol N mol^{-1} electrons in the original condition to between 0.3 and 0.8 mol mol^{-1} in the orgN electrolyte conditions, with the GO_{low} condition having the lowest R_N (0.33 ± 0.02 mol mol^{-1}) and the GO condition having the highest R_N (0.75 ± 0.45 mol mol^{-1})

(Figure 2c). This decrease is likely due to the change in initial available NH_4^+ concentration from the Original to the orgN conditions. For all the orgN conditions, the majority of substrate N was orgN, with readily available NH_4^+ omitted from the substrate entirely in the GO and GO_{low} conditions. Regardless of availability of NH_4^+ in the feed substrate, all final anolyte measurements in orgN conditions indicated the majority of nitrogen was in the form of NH_4^+ (Figure 3). This finding, coupled with measured NH_3-N in the final catholyte solutions for all conditions, indicates the occurance of N mineralization in the anode chamber and subsequent NH_4^+ transfer to the cathode chamber via the CEM. It is inferred that microbes capable of N mineralization were responsible for these reactions, as discussed in section 3.2.1. In the orgN conditions, the microbe-mediated process of N mineralization was a limiting process, meaning it had to occur before NH_4^+ was available for transport across the CEM. This added step resulted in decreased R_N compared to the original condition, in which there was ample NH_4^+ available for transport via the feed anolyte solution. This phenomenon is further discussed in section 3.3.

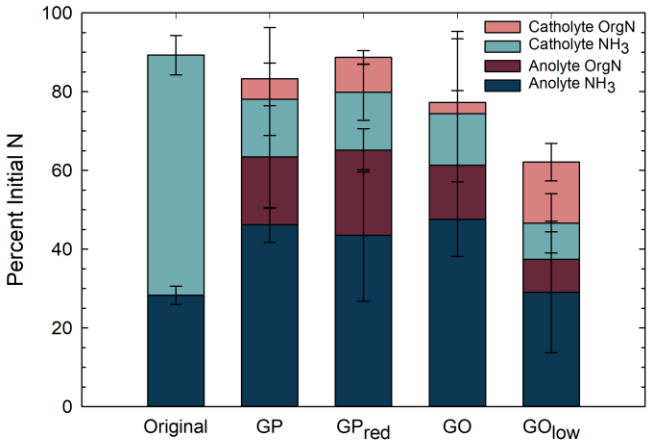

Figure 3. Nitrogen partitioning in final electrolyte solutions as percentages of initial anolyte total nitrogen at different feed conditions. NH_3 is the sum of $NH_{3(aq)}$ and NH_4^+. Organic nitrogen

(OrgN) fractions are omitted for the Original feed condition as all N-addition was as NH_4Cl. Categories along the *x*-axis correspond to feed conditions as outlined in Table 1: the original acetate and NH_4Cl feeding condition ("Original"), a glycine and phosphate buffer anolyte condition ("GP"), a glycine and reduced phosphate buffer condition ("GP_{red}"), a glycine only anolyte condition ("GO"), and an ultra-low glycine only anolyte condition ("GO_{low}").

In the Original electrolyte condition, a baseline anolyte nitrogen removal efficiency of approximately 72% was established. Under orgN electrolyte conditions, anolyte N removal dropped to around 60% for the GO_{low} condition and to around 40% for the GP, GP_{red}, and GO conditions (Figure 3, represented as the difference between 100%, the maximum bar height possible, and the sum of the remaining anolyte N). The majority of N remaining in the anolyte in orgN conditions was NH_3-N, with a maximum of 22 ± 19% of initial N remaining in the anolyte as orgN in the GP_{red} condition. While the majority of nitrogen transferred to the catholyte was NH_3-N, some orgN was observed to have transferred into the catholyte (5.1 ± 4.2% in the GP condition, 8.5 ± 8.8% in the GP_{red} condition, 2.9 ± 2.6% in the GO condition, and 15 ± 3.5% in the GO_{low} condtion). In the GO_{low} condition, this orgN made up the majority of remaining N in the catholyte (Figure 3). Glycine was ruled out as the source of this catholyte orgN through diffusion experiments (Table S2), so it is inferred that the catholyte orgN consists of small degradation intermediates. Future work investigating the speciation of anolyte and catholyte orgN is necessary to fully understand the degradation pathways in the MFC.

3.2. Microbial Community Analysis

Microbial communities collected at five representative cell conditions were analyzed via 16S rRNA sequencing to evaluate changes in anode microbial community structure under varying electrolyte conditions. Sampling conditions included the "Inoculant" anaerobic digestate, the "Initial Electrogens" present directly after resistance decrease to 10 Ohms, and the "Original", glycine only ("GO"), and ultra-low glycine only ("GO_{low}") electrolyte conditions (see Table 1 for descriptions of each condition). Samples from both the GO and GO_{low} conditions were collected at multiple time points throughout the sampling condition, denoted as either "Condition Start", "Mid-condition", or "Condition End". Community composition and structure, as well as alpha and beta diversities, were evaluated.

3.2.1. Community Composition

The top four most abundant phyla across all samples were Bacteroidota (4.7%), Firmicutes (2.2%), Proteobacteria (2.0%), and Halobacterota (1.7%) (Figure 4a). The phyla Bacteriodota, Firmicutes, and Proteobacteria are of the kingdom Bacteria, and all contain organisms capable of electricity generation (Sun et al., 2014; Chen et al., 2016; Yuan et al., 2017; Jin et al., 2018; Liu et al., 2018; Guang et al., 2020; Shi et al., 2021; Li et al., 2022). The phylum Halobacterota is in the kingdom Archaea, and is the phylum of many known methanogenic and methanotrophic microorganisms (Sun et al., 2014). Operation at the Original feed condition, which constituted frequent changing of the electrolyte solutions to replenish depleted COD and nutrient concentrations (as opposed to the infrequent solution changes during the resistance decrease that helped characterize the Initial Electrogens sampling condition), enriched the number of Bacteroidota and Actinobacterota present in the community. Of the organisms of phylum Bacteriodota present, the top three most abundant operational taxonomic units (OTUs) were identified as belonging to the genus *Lentimicrobium*. Organisms of this genus

are known to have electron-dense extracellular polymeric substances (EPS) on their cell surfaces, making them good facilitators of extracellular electron transport (EET) in the anode chamber (Liu et al., 2018). Other prominent Bacteroidota genera identified were *Petrimonas* (protein-degrading, fermentative organisms having known synergistic interactions with exoelectrogenic bacteria), *PHOS-HE36* (sulfur oxidizing bacteria), and *Blvii28* (fermentative organisms with known synergistic interactions with exoelectrogenic bacteria) (Sun et al., 2014; Chen et al., 2016; Shi et al., 2021). The top genus among the organisms of Actinobacteriota present was identified as *Rhodococcus*, a genus of organism responsible for acetate degradation and possessing exoelectrogenic capabilities (Cheng et al., 2018).

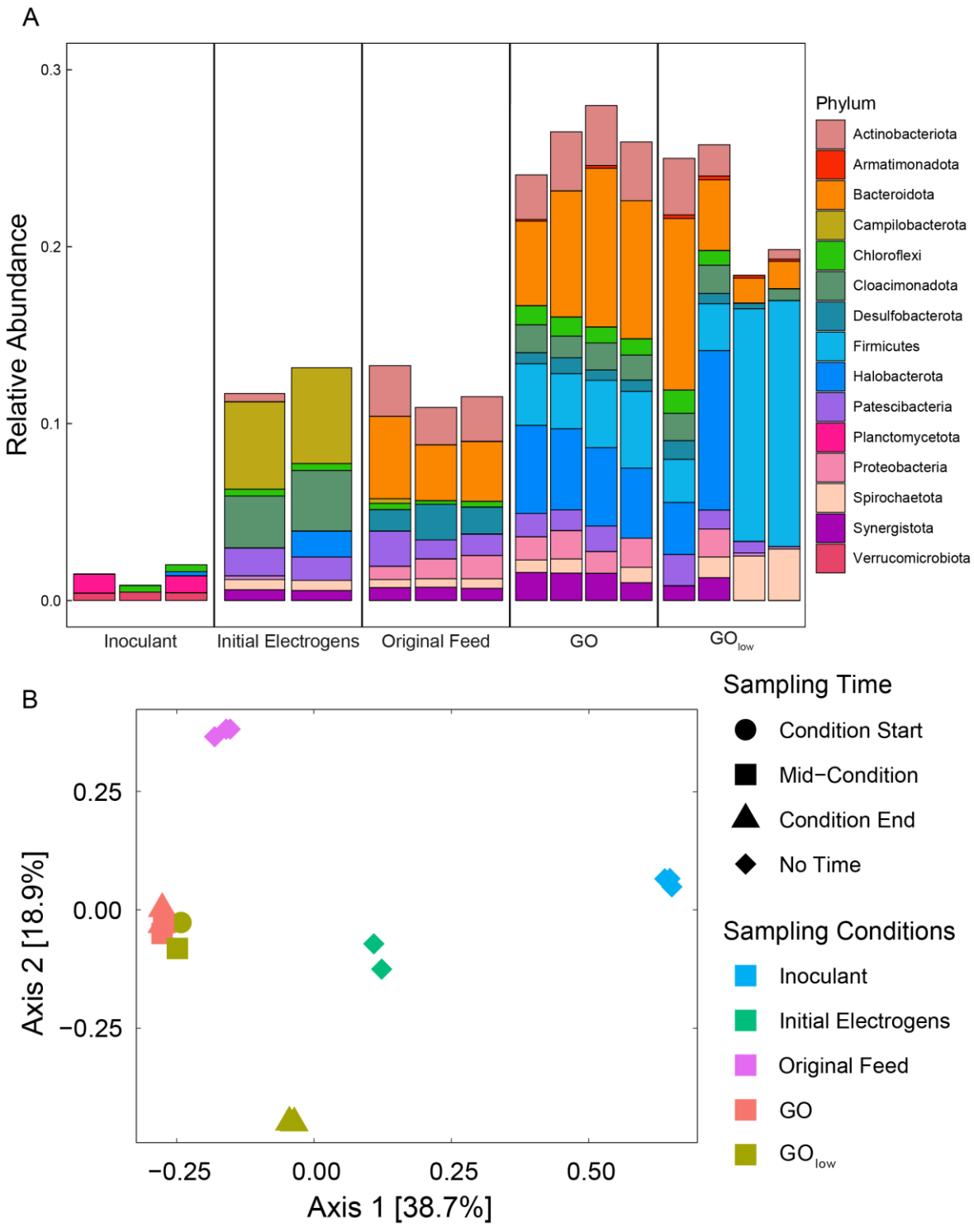

Figure 4. Microbial community analysis for anodic biomass under different feed conditions and at different intra-condition sampling times: (A) relative abundances of the top 15 most abundant phyla across all electrolyte conditions for which biomass samples were collected, and (B)

433 principle coordinate analysis (PCoA) comparing community diversities for different electrolyte
434 conditions and intra-condition sampling times. Sampling Conditions are as follows: “Inoculant”
435 indicates the community in the mesophilic anaerobic sludge used to inoculate the MFC, “Initial
436 Electrogens” indicates the community present directly following resistance decrease to 10 Ω,
437 “Original Feed” indicates the community present after several experimental cycles were
438 completed at the original acetate and NH_4Cl feed condition (see Table 1), “GO” indicates the
439 community present during and after several experimental cycles at the glycine only (GO) feed
440 conditions (see Table 1), and “GO_{low}” indicates the community present during and after several
441 experimental cycles at the ultra-low glycine only (GO_{low}) feed condition (see Table 1). Sampling
442 Time denotes the relative time within the specific Sampling Condition of the community sample
443 collection; prior to the start of the Sampling Condition (“Condition Start”), during the course of
444 the Sampling Condition (“Mid-condition”), or directly after the completion of the Sampling
445 Condition (“Condition End”). Samples indicated as having “No Time” denote those that were
446 collected in replicate at only one time. PCoA is based on Bray-Curtis dissimilarity. Community
447 composition data was obtained via 16S rRNA sequencing. Graphic prepared using the “ggplot2”
448 package in R (Wickham, 2016; Team, 2022).

449 Under orgN conditions (e.g. GO and GO_{low}), organisms of phyla Bacteroidota and
450 Actinobacteriota continue to persist, but decrease in number towards the end of the GO_{low}
451 condition (Figure 4a). Instead, the phylum Firmicutes emerges as an increasingly dominant
452 group. Of the Firmicutes present, organisms belonging to the genera *Bacillus* are the most
453 abundant. *Bacillus* organisms are known to facilitate N mineralization, which converts orgN to
454 inorganic nitrogen, usually NH_4^+ (Mandic-Mulec et al., 2016). Furthermore, members of the
455 phylum Firmicutes have been shown to exhibit exoelectrogenic capabilities (Wrighton et al.,

2008; Zhou et al., 2019). It is possible that the decrease in abundance of Bacteriodota and Actinobactriota phyla and corresponding increase in relative abundance of Firmicutes phyla indicates a selection for organisms capable of both exoelectrogenic and nitrogen mineralizing abilities as the conditions increasingly select for both capabilities.

Interestingly, the presence of the phyla Campilobacterota, a known sulfate oxidizer which can use nitrate as an electron acceptor, is unique to the initial electrogenic community. This indicates that, under the imposed selection pressures for electrogenic N mineralizers, the need for sulfate oxidation is diminished (Begmatov et al., 2021). Furthermore, the phylum Cloacimonadota, while present under both GO and GO_{low} conditions, decreases in relative abundance as selection pressures are increased from the initial electrogenic community to that present under the GO_{low} condition (Figure 4a). Cloacimonadota contains members known to perform propionate oxidation, and decreased numbers of Cloacimonadota in anaerobic digestion processes are suggested to indicate instability due to increasing NH_3-N concentrations (Bi et al., 2020; Christou et al., 2021). As NH_3-N production is a desired outcome of this research, the decrease in Cloacimonadota organisms is a promising finding.

3.2.2. Diversity Metrics

Alpha diversity of each sample was calculated using Shannon diversity (Eq. 3) for the richness of a microbial community; for the inoculant, initial electrogenic, and original feed communities, Shannon diversity was equal to 2.11, dropped to 2.08 for the community present during the GO condition, and then varied from 2.11 at the start of the GO_{low} condition to 2.02 at the end of the experimental cycles in this condition. Statistical analyses revealed that the initial electrogenic community was the only community where the electrolyte condition was not a statistically significant predictor of Shannon diversity (p-value = 0.346). Interestingly, when

tested against only the GO condition samples, the samples from the end of the GO_{low} condition were not significant predictors of Shannon diversity (p-value = 0.593), despite the large difference in calculated Shannon diversities (2.08 for GO samples versus 2.02 for GO_{low} samples at the end of the condition). The generally decreasing trend in the Shannon diversity of samples as the electrolyte conditions progress from unchanged inoculant to highly cultivated orgN conditions (i.e. GO and GO_{low}) suggests that the changes in electrolyte compositions permitted cultivation of an increasingly specific microbial community. The comparatively large Shannon diversity of the initial GO_{low} community warrants further research and evaluation.

Figure 4b presents a principle coordinate analysis (PCoA) based on Bray-Curtis dissimilarity metrics comparing the community diversities for different electrolyte conditions (color) and intra-condition sampling times (marker shape), with both axis representing > 57% of total dissimilarity. The majority of the sampling conditions tested present as highly clustered and distinctly different, indicating distinct communities in each sampling condition. For the GO and GO_{low} conditions, multiple samples were collected at various time points within the sampling condition. In the GO sampling condition, the microbial community showed no change in respect to intra-condition sampling time, indicated by the clustering of the GO sample points in Figure 4b. For the GO_{low} condition, the microbial community differed from the beginning and middle to the end of the sampling condition, as indicated by the split clustering for this condition at different time points in Figure 4b. This split clustering is further evidence of community adaptation to varying conditions, as is discussed in section 3.3.

3.3. Microbial degradation pathways under differing electrolyte conditions

The electrolyte condition had significant effects on the MFC's nutrient removal efficiency, leading to several key inferences regarding the microbial degradation pathways for

organic matter in different conditions. Of specific interest are the total and NH_3-N concentrations measured in initial and final electrolyte solutions while the MFC was operated in the GO_{low} condition. Figure 5 shows the difference in TN removed from the anolyte and accumulated in the catholyte for nine separate experimental cycles in the GO_{low} condition. Cycles 1 and 2 have final anolyte TN concentrations higher than that of the initial anolyte solution (Figure S2), implying an increase of TN within the system. Furthermore, the final NH_3-N concentration is greater than that of the initial NH_3-N concentration in only 4 of the 9 cycles at this condition (Figure S2), in contradiction to the hypothesis that, with no other form of N provided, orgN (in the form of glycine) will be degraded to NH_4^+, thus increasing NH_3-N concentration from initial to final measurements. Additionally, cycles 1, 2, 5, and 6 exhibited excessive accumulation of catholyte TN throughout the cycle, meaning that the amount of TN accumulated in the catholyte was greater than that which was removed from the anolyte (Figure 5). Based on how samples were collected and analyzed, which included a filtration step prior to measuring the nutrient concentrations for all solutions, it is inferred that this excess N, which appears in the catholyte as both NH_3-N and orgN, is N that was previously contained within microbial cells. We infer that this release of N occurred due to a combination of system instability and ultra-low concentrations of available N in the anolyte. The early cycles in the GO_{low} condition (cycle 1-6) saw fluctuations in TN and NH_3-N removal and accumulation as the system worked to re-establish equilibrium after the changed condition. This instability was compounded by the low concentration of available orgN which characterized the GO_{low} condition, as it led to cell death and lysis, releasing more organic matter and orgN into the system and pushing it further from an equilibrium state (Figure 6). The proposed microbial metabolism and its impacts on MFC operation are discussed further below.

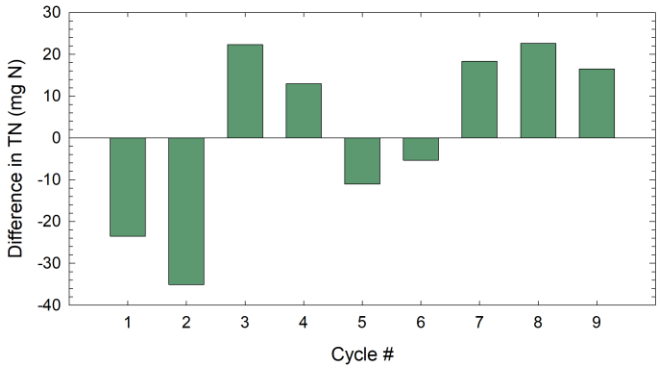

Figure 5. Difference between TN removed from the anolyte and that accumulated in the catholyte for experimental cycles in the ultra-low concentration glycine only (GO_{low}) condition. Negative values indicate higher accumulated catholyte N than removed anolyte N, based on measurements of filtered samples.

Figure 6 depicts the suspected pathways for microbial degredation of orgN and acetate in representative electrolyte feed conditions. Under the original feed condition (Figure 6a), acetate degradation to carbon dioxide (CO_2) and a small quantity of partially-degraded intermediates is the main source of electron generation, while NH_4^+ in the anolyte feed is transferred to the cathode chamber to maintain the charge neutrality. Under the GP_{red} condition (Figure 6b), acetate degradation is still the main source of electron production for current generation, but glycine degredation to NH_4^+ and orgN intermediates also contributes a small portion of current. We note that NH_4^+ produced from orgN degredation also contributes to the NH_4^+ flux from anolyte to catholyte. The GO condition (Figure 6c) is the same, except for the omission of readily available NH_4^+ in the anolyte feed solution, making all available N for electro-driven transport a product of microbe-mediated degredation. Finally, in the GO_{low} condition (Figure 6d), competition for scarce orgN resources leads to cell death on the anode brush. This microbial necromass

represents an additional source of organic matter, specifically orgN, for the active microbes, and is preferentially degraded as an N source over the complex and scarce glycine orgN provided in the feed. The NH_4^+ and orgN intermediates produced from the degradation of microbial necromass are measured in the final solution characteristics, but did not appear in the initial solution measurements due to a filtration step. Thus, the preferential degradation of microbial necromass shows as an overall increase in nitrogen within the MFC at ultra-low orgN conditions (Figure 5).

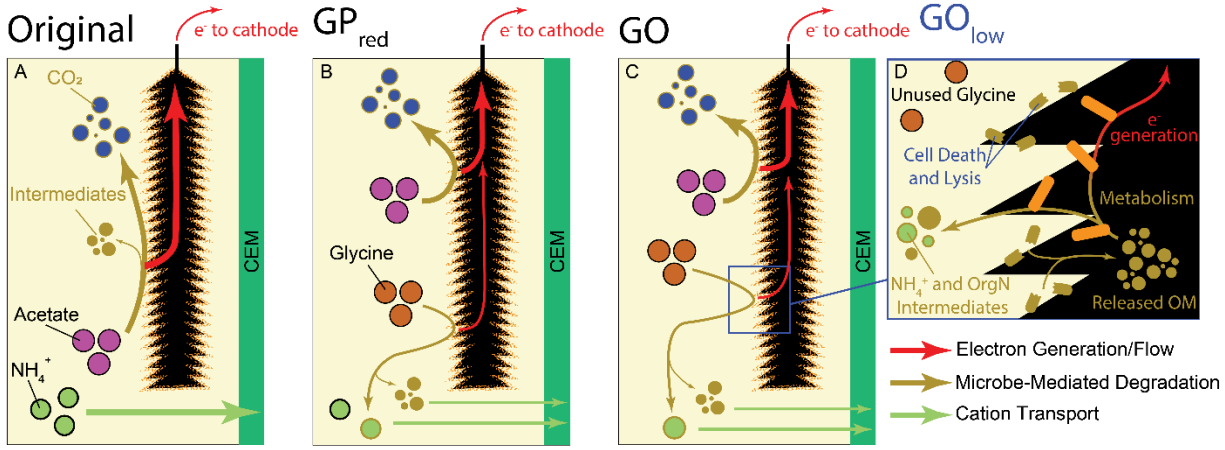

Figure 6. Schematic representation of anodic microbial processes occurring under selected representative feed conditions: (A) the Original acetate and NH_4Cl feed condition (see Table 1), where current generation was solely the result of acetate degradation and NH_4^+ transport was physically/chemically mediated; (B) the glycine and reduced phosphate buffer (GP_{red}) condition (see Table 1) where orgN as glycine was introduced and it's degradation contributed to both the current generation and the mediation of NH_4^+ transport; (C & D) the glycine only (GO) and ultra-low glycine only (GO_{low}) conditions (see Table 1), respectively, where orgN was the only N-source and it's degradation contributed to current generation and was the main mediator of

559 NH_4^+ transport, or, in the GO_{low} condition, was unused in preference of easily-degradable
560 microbial necromass and released organic matter (OM). Chemical components added as part of
561 the anolyte feed solution at the given condition are indicated in black outlines and chemical
562 components produced through microbial metabolism are indicated in brown outlines.

563

564 **4. Conclusions**

565 Microbial fuel cells are considered a promising technology for NH_3 recovery from dairy
566 manure as they can convert the orgN fraction into NH_4^+ and also recover this NH_4^+ as NH_3
567 fertilizer. This work specifically investigated the impacts of various anolyte feed compositions
568 on the MFC's ability to recover NH_3 from orgN. We demonstrate that MFCs operated for NH_3
569 recovery can achieve similar performance to those operated for electricity generation, with the
570 added benefit of recovering NH_3 from the orgN fraction of a synthetic dairy manure. This work
571 also provides insight to the microbial degradation pathways governing orgN to NH_4^+ conversion
572 in MFCs fed with synthetic dairy manure. The findings in this research can be used to inform
573 future work regarding optimizing MFC conditions for orgN to NH_4^+ conversion in the anode
574 chamber and NH_4^+ transport from anode to cathode chambers. Namely, it is important to balance
575 the feed concentration of orgN, as it is shown that low orgN concentration can lead to
576 preferential degradation of microbial biomass for N instead of from converting orgN in manure
577 to NH_4^+.

578 **Declaration of Interests**

579 The authors declare that they have no known competing financial interests or personal
580 relationships that could have appeared to influence the work reported in this paper.

Acknowledgements

The authors would like to thank the support from National Science Foundation CBET 2219089. In addition, the authors would like to thank the startup fund from the Department of Civil and Environmental Engineering, College of Engineering, the Office of the Vice-Chancellor for Research and Graduate Education (OVCRGE) at the University of Wisconsin–Madison, and the Wisconsin Alumni Research Foundation (WARF) for the support of this study. The authors thank the Next Generation Sequencing Core Facility of the Biotechnology Center at UW–Madison for performing library preparation and DNA sequencing, and Sailendharan Sudakaran of the Microbiome Hub and **UW Biotechnology Center Bioinformatics Resource Center** for assistance with sequencing data analysis. The authors gratefully acknowledge the support from Jackie Cooper of the Environmental Engineering Core Facility at the University of Wisconsin–Madison and use of facilities and equipment. We also thank Abigail Monahan for her contributions to the microbial community analysis portion of this work supported by Water@UW-Madison/Fresh Water Collaborative of Wisconsin Undergraduate Research Experience. Finally, the authors thank Christina Segar for her assistance in creation of graphics and icons used in some of the figures presented in this work.

598 Angenent, L.T., Sung, S., 2001. Development of anaerobic migrating blanket reactor (AMBR), a
599 novel anaerobic treatment system. Water Res. 35, 1739-1747.
600 Begmatov, S., Savvichev, A.S., Kadnikov, V.V., Beletsky, A.V., Rusanov, I.I., Klyuvitkin, A.A.,
601 Novichkova, E.A., Mardanov, A.V., Pimenov, N.V., Ravin, N.V., 2021. Microbial
602 Communities Involved in Methane, Sulfur, and Nitrogen Cycling in the Sediments of the
603 Barents Sea. Microorganisms 9, 2362.
604 Bi, S., Westerholm, M., Qiao, W., Xiong, L., Mahdy, A., Yin, D., Song, Y., Dong, R., 2020.
605 Metabolic performance of anaerobic digestion of chicken manure under wet, high solid, and
606 dry conditions. Bioresour. Technol. 296, 122342.
607 Bray, J.R., Curtis, J.T., 1957. An Ordination of the Upland Forest Communities of Southern
608 Wisconsin. Ecol. Monogr. 27, 325-349.
609 Chen, Y., Chen, M., Shen, N., Zeng, R.J., 2016. H2 production by the thermoelectric
610 microconverter coupled with microbial electrolysis cell. Int. J. Hydrog. Energy 41, 22760-
611 22768.
612 Cheng, P., Shan, R., Yuan, H.-R., Deng, L.-f., Chen, Y., 2018. Enhanced Rhodococcus
613 pyridinivorans HR-1 anode performance by adding trehalose lipid in microbial fuel cell.
614 Bioresour. Technol. 267, 774-777.
615 Cheng, S., Dempsey, B.A., Logan, B.E., 2007. Electricity Generation from Synthetic Acid-Mine
616 Drainage (AMD) Water using Fuel Cell Technologies. Environ. Sci. Technol. 41, 8149-8153.
617 Christou, M.L., Vasileiadis, S., Kalamaras, S.D., Karpouzas, D.G., Angelidaki, I., Kotsopoulos,
618 T.A., 2021. Ammonia-induced inhibition of manure-based continuous biomethanation
619 process under different organic loading rates and associated microbial community dynamics.
620 Bioresour. Technol. 320, 124323.
621 Chu, N., Liang, Q., Jiang, Y., Zeng, R.J., 2020. Microbial electrochemical platform for the
622 production of renewable fuels and chemicals. Biosensors Bioelectron. 150, 111922.
623 Cord-Ruwisch, R., Law, Y., Cheng, K.Y., 2011. Ammonium as a sustainable proton shuttle in
624 bioelectrochemical systems. Bioresour. Technol. 102, 9691-9696.
625 De Paepe, J., De Paepe, K., Gòdia, F., Rabaey, K., Vlaeminck, S.E., Clauwaert, P., 2020. Bio-
626 electrochemical COD removal for energy-efficient, maximum and robust nitrogen recovery
627 from urine through membrane aerated nitrification. Water Res. 185, 116223.
628 EPA, U., 2008. The Clean Water Act. in: EPA, U. (Ed.). 33.
629 EPA, U., 2022. NPDES CAFO Permitting Status Report: Endyear 2020. US EPA.
630 Gil, G.-C., Chang, I.-S., Kim, B.H., Kim, M., Jang, J.-K., Park, H.S., Kim, H.J., 2003.
631 Operational parameters affecting the performannce of a mediator-less microbial fuel cell.
632 Biosensors Bioelectron. 18, 327-334.
633 Guang, L., Koomson, D.A., Jingyu, H., Ewusi-Mensah, D., Miwornunyuie, N., 2020.
634 Performance of Exoelectrogenic Bacteria Used in Microbial Desalination Cell Technology.
635 Int. J. Env. Res. Public Health 17, 1121.
636 Gude, V.G., 2016. Wastewater treatment in microbial fuel cells – an overview. J. Clean. Prod.
637 122, 287-307.
638 Gul, M.M., Ahmad, K.S., 2019. Bioelectrochemical systems: Sustainable bio-energy
639 powerhouses. Biosensors Bioelectron. 142, 111576.
640 Hansen, K.H., Angelidaki, I., Ahring, B.K., 1998. ANAEROBIC DIGESTION OF SWINE
641 MANURE: INHIBITION BY AMMONIA. Water Res. 32, 5-12.

He, Z., Huang, Y., Manohar, A.K., Mansfeld, F., 2008. Effect of electrolyte pH on the rate of the anodic and cathodic reactions in an air-cathode microbial fuel cell. Bioelectrochemistry 74, 78-82.
Jin, X., Guo, F., Liu, Z., Liu, Y., Liu, H., 2018. Enhancing the Electricity Generation and Nitrate Removal of Microbial Fuel Cells With a Novel Denitrifying Exoelectrogenic Strain EB-1. Front. Microbiol. 9.
Kelly, P.T., He, Z., 2014. Nutrients removal and recovery in bioelectrochemical systems: A review. Bioresour. Technol. 153, 351-360.
Kim, K.-Y., Moreno-Jimenez, D.A., Efstathiadis, H., 2021. Electrochemical Ammonia Recovery from Anaerobic Centrate Using a Nickel-Functionalized Activated Carbon Membrane Electrode. Environ. Sci. Technol. 55, 7674-7680.
Kuntke, P., Śmiech, K.M., Bruning, H., Zeeman, G., Saakes, M., Sleutels, T.H.J.A., Hamelers, H.V.M., Buisman, C.J.N., 2012. Ammonium recovery and energy production from urine by a microbial fuel cell. Water Res. 46, 2627-2636.
Li, J., Yao, C., Song, B., Zhang, Z., Brock, A.L., Trapp, S., Zhang, J., 2022. Regulating Sulfate-Reducing and Sulfur-Oxidizing Bacteria via S-doped NiFe2O4 nanosheets as Microbial Fuel Cell anode for simultaneous enhancement of sulfer and energy recovery.
Liu, D., Wang, R., Chang, W., Zhang, L., Peng, B., Li, H., Liu, S., Yan, M., Guo, C., 2018. Ti3C2MXene as an excellent anode material for high-performance microbial fuel cells. J. Mater. Chem. A 6, 20887-20895.
Liu, H., Ramnarayanan, R., Logan, B.E., 2004. Production of Electricity during Wastewater Treatment Using a Single Chamber Microbial Fuel Cell. Environ. Sci. Technol. 38, 2281-2285.
Liu, Y., Qin, M., Luo, S., He, Z., Qiao, R., 2016. Understanding Ammonium Transport in Bioelectrochemical Systems towards its Recovery. Sci. Rep. 6, 22547.
Logan, B.E., Hamelers, B., Rozendal, R., Schröder, U., Keller, J., Freguia, S., Aelterman, P., Verstraete, W., Rabaey, K., 2006. Microbial Fuel Cells: Methodology and Technology†. Environ. Sci. Technol. 40, 5181-5192.
Long, C.M., Muenich, R.L., Kalcic, M.M., Scavia, D., 2018. Use of manure nutrients from concentrated animal feeding operations. J. Great Lakes Res. 44, 245-252.
Lu, L., Ren, Z.J., 2016. Microbial electrolysis cells for waste biorefinery: A state of the art review. Bioresour. Technol. 215, 254-264.
Mandic-Mulec, I., Stefanic, P., van Elsas, J.D., 2016. Ecology of Bacillaceae. The Bacterial Spore, pp. 59-85.
McMurdie, P.J., Holmes, S., 2013. phyloseq: An R Package for Reproducible Interactive Analysis and Graphics of Microbiome Census Data. PLoS ONE 8, e61217.
Pant, D., Van Bogaert, G., Diels, L., Vanbroekhoven, K., 2010. A review of the substrates used in microbial fuel cells (MFCs) for sustainable energy production. Bioresour. Technol. 101, 1533-1543.
Pardo, G., Moral, R., Aguilera, E., Del Prado, A., 2015. Gaseous emissions from management of solid waste: a systematic review. Global Change Biol. 21, 1313-1327.
Qin, M., He, Z., 2014. Self-Supplied Ammonium Bicarbonate Draw Solute for Achieving Wastewater Treatment and Recovery in a Microbial Electrolysis Cell-Forward Osmosis-Coupled System. Environ. Sci. Technol. Lett. 1, 437-441.

686 Qin, M., Liu, Y., Luo, S., Qiao, R., He, Z., 2017. Integrated experimental and modeling
687 evaluation of energy consumption for ammonia recovery in bioelectrochemical systems.
688 Chem. Eng. J. 327, 924-931.
689 Qin, M., Molitor, H., Brazil, B., Novak, J.T., He, Z., 2016. Recovery of nitrogen and water from
690 landfill leachate by a microbial electrolysis cell–forward osmosis system. Bioresour.
691 Technol. 200, 485-492.
692 Rasouli Sadabad, H., Badalians Gholikandi, G., 2018. Simultaneous effective sludge
693 stabilization and direct electricity generation by merging microbial fuel cell (MFC) and
694 Fered-Fenton reactor: An experimental study. Biomass Bioenergy 119, 75-89.
695 Ren, Z., Steinberg, L.M., Regan, J.M., 2008. Electricity production and microbial biofilm
696 characterization in cellulose-fed microbial fuel cells. Water Sci. Technol. 58, 617-622.
697 Ren, Z., Ward, T.E., Regan, J.M., 2007. Electricity Production from Cellulose in a Microbial
698 Fuel Cell Using a Defined Binary Culture. Environ. Sci. Technol. 41, 4781-4786.
699 Rodríguez Arredondo, M., Kuntke, P., Jeremiasse, A.W., Sleutels, T.H.J.A., Buisman, C.J.N.,
700 Ter Heijne, A., 2015. Bioelectrochemical systems for nitrogen removal and recovery from
701 wastewater. Environ. Sci. Water Res. Technol. 1, 22-33.
702 Rodríguez Arredondo, M., Kuntke, P., Ter Heijne, A., Hamelers, H.V.M., Buisman, C.J.N.,
703 2017. Load ratio determines the ammonia recovery and energy input of an electrochemical
704 system. Water Res. 111, 330-337.
705 Rozendal, R.A., Leone, E., Keller, J., Rabaey, K., 2009. Efficient hydrogen peroxide generation
706 from organic matter in a bioelectrochemical system. Electrochem commun 11, 1752-1755.
707 Shi, C., Xu, Y., Liu, M., Chen, X., Fan, M., Liu, J., Chen, Y., 2021. Enhanced bisphenol S
708 anaerobic degradation using an NZVI–HA-modified anode in bioelectrochemical systems. J.
709 Hazard. Mater. 403, 124053.
710 Smith, C., Hill, A.K., Torrente-Murciano, L., 2020. Current and future role of Haber–Bosch
711 ammonia in a carbon-free energy landscape. Energy Environ. Sci. 13, 331-344.
712 Sun, R., Xing, D., Jia, J., Liu, Q., Zhou, A., Bai, S., Ren, N., 2014. Optimization of high-solid
713 waste activated sludge concentration for hydrogen production in microbial electrolysis cells
714 and microbial community diversity analysis. Int. J. Hydrog. Energy 39, 19912-19920.
715 Syed, Z., Sonu, K., Sogani, M., 2022. Cattle manure management using microbial fuel cells for
716 green energy generation. Biofuel Bioprod Biorefin 16, 460-470.
717 Team, R.C., 2022. R: A language and environment for statistical computing. R Foundation for
718 Statistical Computing, Vienna, Austria.
719 Wang, H., Ren, Z.J., 2013. A comprehensive review of microbial electrochemical systems as a
720 platform technology. Biotechnol. Adv. 31, 1796-1807.
721 Wang, M., Khan, M.A., Mohsin, I., Wicks, J., Ip, A.H., Sumon, K.Z., Dinh, C.-T., Sargent, E.H.,
722 Gates, I.D., Kibria, M.G., 2021. Can sustainable ammonia synthesis pathways compete with
723 fossil-fuel based Haber–Bosch processes? Energy Environ. Sci. 14, 2535-2548.
724 Wickham, H., 2016. ggplot2: Elegant Graphics for Data Analysis. Springer-Verlag New York,
725 New York.
726 Willis, A., Martin, B.D., 2022. DivNet: Diversity Estimation in Networked Ecological
727 Communities.
728 Wrighton, K.C., Agbo, P., Warnecke, F., Weber, K.A., Brodie, E.L., Desantis, T.Z., Hugenholtz,
729 P., Andersen, G.L., Coates, J.D., 2008. A novel ecological role of the Firmicutes identified in
730 thermophilic microbial fuel cells. ISME J 2, 1146-1156.

731 Yang, Y., Qin, M., Yang, X., He, Z., 2017. Enhancing hydrogen production in microbial
732 electrolysis cells by in situ hydrogen oxidation for self-buffering pH through periodic
733 polarity reversal. Journal of Power Sources 347, 21-28.
734 Ye, Y., Ngo, H.H., Guo, W., Liu, Y., Chang, S.W., Nguyen, D.D., Ren, J., Liu, Y., Zhang, X.,
735 2019. Feasibility study on a double chamber microbial fuel cell for nutrient recovery from
736 municipal wastewater. Chem. Eng. J. 358, 236-242.
737 Yuan, H., Sun, S., Abu-Reesh, I.M., Badgley, B.D., He, Z., 2017. Unravelling and
738 Reconstructing the Nexus of Salinity, Electricity, and Microbial Ecology for
739 Bioelectrochemical Desalination. Environ. Sci. Technol. 51, 12672-12682.
740 Zhang, E., Liu, L., Cui, Y., 2012. Effect of pH on the performance of the anode in microbial fuel
741 cells. Adv Mat Res 608-609, 884-888.
742 Zhang, F., Ge, Z., Grimaud, J., Hurst, J., He, Z., 2013. Long-Term Performance of Liter-Scale
743 Microbial Fuel Cells Treating Primary Effluent Installed in a Municipal Wastewater
744 Treatment Facility. Environ. Sci. Technol. 47, 4941-4948.
745 Zhang, F., Li, J., He, Z., 2014. A new method for nutrients removal and recovery from
746 wastewater using a bioelectrochemical system. Bioresour. Technol. 166, 630-634.
747 Zhou, H., Mei, X., Liu, B., Xie, G., Xing, D., 2019. Magnet anode enhances extracellular
748 electron transfer and enrichment of exoelectrogenic bacteria in bioelectrochemical systems.
749 Biotechnol. Biofuels 12.